Static Bending, Vibration, and Buckling Responses of a Sandwich Beam Composed of Five Layers Considering Honeycomb Core and CNTRC with SMA Particles and Temperature-Dependent Material Properties Using SSDT

Mohsen Asgari, Mehdi Mohammadimehr*, Mohammad Arabzadeh-Ziari, Erfan Arabzadeh-Ziari

Department of Solid Mechanics, Faculty of Mechanical Engineering, University of Kashan, Kashan 87317-53153, Iran P.O.

**Corresponding Author: Professor, Email:* mmohammadimehr@kashanu.ac.ir

ARTICLE INFO

Article history:

Received:
Revised:
Accepted:

Keywords:

CNT/SMA reinforced composite face sheets;
honeycomb core;
Sinusoidal shear deformation theory;
A five layers sandwich beam;
Static bending, vibration, and buckling;

ABSTRACT

The novelty and main contributions of this research are to investigate simultaneously static bending, free vibration, and buckling responses of a sandwich beam composed of a five-layer beam using sinusoidal shear deformation theory (SSDT). In this work, five layers of a sandwich beam including a honeycomb core, carbon nanotubes reinforced composite (Matrix and Resin) (CNTRC) at the top and bottom of the core, and also, shape memory alloy (SMA) in the form of nanoscale particles with matrix in top and bottom of CNTRC are derived. In this study, the governing equations of equilibrium are obtained using the principle of minimum potential energy for deflection and buckling analyses, while Hamilton's principle is employed to obtain the governing equations of motion. Then, based on Navier's type method for simply supported boundary conditions, the deflection, critical buckling load, and the natural frequency for a sandwich beam composed of five layers are obtained. To validate the results, they are compared with existing literature, and there is a good agreement between them. Also, the effects of the thickness of the core, volume fraction of carbon nanotubes, and volume fraction of SMA are analyzed. The results reveal that changing the volume fraction from 0 to 0.01 results in a 30% decrease in deflection. It is concluded that with an enhancement in thickness ratio, the heat flux decreases due to the increase in the thickness of the core, while the thickness of face sheets decreases because the conductivity coefficient for CNT is higher than the core. Moreover, increasing temperature softens the material, leading to a decrease in the critical buckling load.

1. Introduction

The sandwich structures consist of two thin face sheet layers with high strength and a thick, low-density core layer to achieve excellent properties. In the military and aerospace industries, it is very important to design a structure resistant to blast and impact loads[1–13]. Ghorbanpour Arani et al. [6] studied the free and forced vibrations of double viscoelastic piezoelectric nanobeam systems (DVPNBSs) using nonlocal viscoelasticity theory and the Euler–Bernoulli beam model.

Also, some technical expressions on the application of a sandwich beam are extensively used in aerospace, automotive, civil, marine, drone, and other high-performance structures because of their high specific stiffness and strength, excellent fatigue resistance, long durability, and many other superior properties compared to the conventional metallic materials [14–17].

1.1 *Structures and Applications of Carbon Nanotube*

Carbon nanotubes have high strength and good thermal and electrical properties[18–21]. Currently, composites with carbon nanotube particles are used to construct aircraft bodies, transmission pipes, and Transistors[22, 23]. Also, functionally graded carbon nanotube (FG-CNT) is used in medical science as a platform for drug delivery [24–29]. Garg et al. [30] studied the vibration and bending analyses of FG-CNT reinforced composite (FG-CNTRC) for a sandwich beam. Ghorbanpour Arani et al. [31] investigated the vibration and instability of visco-elastically coupled CNTRC microtubes conveying fluid. Li et al. [32] investigated the effect of adding carbon nanotubes on the behavior of the structure by enhancing the

volume fraction (V) of CNTs, and the strength of the composite increases. Excessive V-CNT has led to a decrease in strength. Zhang et al. [33] added carbon nanotubes to polymer materials to improve the mechanical properties of composites. Their experimental results have shown that epoxy composites reinforced by CNTs with a length of 5 to 20 micrometers have greater strength and toughness than shorter CNTs of 0.5 to 2 micrometers. Arshadi et al. [34] studied the vibration and bending of a sandwich microbeam with a functionally graded porous core (FG) and two polymer plates reinforced with graphene nanoplatelets (GPLs). Their results showed that the VA distribution type has the highest deviation, and the AV type has the lowest static bending value. Ghorbanpour Arani et al. [35] analyzed the stress of a long piezoelectric polymer hollow cylinder reinforced with carbon nanotubes under magnetic and mechanical loadings. The results showed that increasing V-CNTs increases the strength of the nanocomposite cylinder. Also, carbon nanotubes increase bending resistance and fracture toughness [36, 37]. Ghorbanpour Arani et al. [38] investigated the nonlinear dynamic analysis of an embedded functionally graded sandwich nanobeam (FGSNB) with integrated magnetically restrained layers. They concluded that the magnetic layers significantly affect the dynamic behavior of FGMSNB. Arefi et al. [39–41] investigated the free vibration analysis of a three-layer microbeam consisting of an elastic microcore and two piezomagnetic plates, which are located on the Pasternak base. Their results showed that the increase of three microscale parameters significantly increased three natural frequencies. Arefi et al. [42] studied the buckling and free vibration analyses of a sandwich beam comprised of softcore and functionally graded graphene platelets (GPLs) reinforced composite face sheets.

1.2 *Smart Structures and Applications of SMA*

Shape-memory alloys are metals used for smart structures, such as KTS-SM alloy, one of the most reliable Ni-Ti alloys. KTS-SM alloy is used in the construction of hot water shut-off valves for water purification, evaporative emission control systems, dental implants, and fire dampers [43, 44]. Asadi et al. [45] analyzed the post-buckling behavior of multilayer beams with memory alloy under uniform heating. The fibers of this alloy are very effective at delaying the heat flux in the beam. The results have shown that increased fiber volume fraction or fiber prestressing increases the strain temperature. Alambeigi et al. [46] investigated forced vibration for a sandwich beam with FG porous core and composite layers embedded with SMA. Their numerical results have shown that with the increase in the volume fraction of memory alloys, the dimensionless natural frequency increases. Vishal et al. [47] investigated active control of vibration based on SMA as an actuator. Garafolo and McHugh [48] illustrated the effect of SMA in reducing vibration produced by aeroelastic flutter. Their results show that activating the embedded SMA wire leads to enhanced stiffness and a decrease in the vibration amplitude of the flutter. Rocha et al. [49] studied the post-tensioning mechanical feasibility of annealed glass beams by activating Fe-SMA reinforcement with external bonding. Zheng et al. [50] researched the reverse effect of shape memory alloys. They concluded that the shape memory alloy has a maximum reverse effect of 1.63%. Viet et al. [51] researched porous composite beams, including the FGP SMA layer. Their results showed that increasing the thickness of the SMA layer increases energy absorption. Lu et al. [52] investigated the method of improving the dynamic stiffness of structures at high temperatures with SMA actuators. Samadpour et al. [53] studied the vibration of thermally buckled SMA hybrid composite sandwich plates. Park et al. [54] research was done on the vibration of thermally post-buckled composite plates embedded with SMA. Their numerical results showed that using SMA increases the critical temperature. Kuang et al. [55] used optical fiber sensors to actively control smart composites with shape memory alloy sheets. Khalili et al. [56] studied the bending properties of composites reinforced with SMA wires. Their results showed that the pre-strained wires caused a 13% increase in the maximum bending load. Nejati et al. [57] analyzed the thermal vibration of composite reinforced with SMA wires. Their results showed that SMA wires increase the thermal frequency.

This work's main contributions and novelty are to consider simultaneously static bending, free vibration, and buckling responses of a sandwich beam composed of a five-layer beam using sinusoidal shear deformation theory (SSDT). In this work, a sandwich beam composed of five layers including a honeycomb core, carbon nanotubes reinforced composite (CNTRC) at the top and bottom of the core, and also shape memory alloy (SMA) in the form of nanoscale particles with matrix on top and bottom of CNTRC is obtained. Moreover, it must be explained that employing two types of nanoparticles: SMA is known for its smart material properties, and CNT is used as reinforcement in composite structures. This study derives the governing equations of equilibrium using the principle of minimum potential energy for deflection and buckling analyses, while Hamilton's principle is employed to obtain the governing equations of motion and

then the natural frequencies of a sandwich beam. The obtained results investigate the influence of the core thickness, volume fraction of carbon nanotube particles, and SMA on the deflection, frequency, and buckling of a sandwich beam.

2. Mathematical Modeling

Figure 1 shows the sandwich beam consists of a honeycomb core and two nanocomposite face sheets reinforced by CNT/Epoxy/fiber and SMA. To derive a mathematical model of the sandwich beam, the used assumptions and modifications are presented as follows:

- The sandwich structure is assumed to be in the elastic region. Thus, Hook's law becomes correct.
- The top and bottom layers of cores have the same properties.
- It is assumed that the core and face sheets are fully bonded. Therefore, there is no slippage at the interfaces between the core and face sheets.
- For every point on a cross-section, the displacement fields are the same.
- In this research, the two-end boundary conditions are assumed to be simply supported, and the governing equations of motion are solved using Navier's type method.

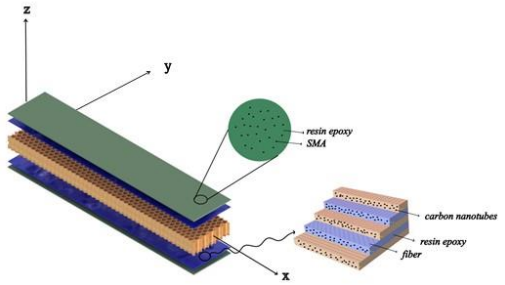

Fig.1. A schematic view of a sandwich beam composed of five layers

Young's modulus is calculated using the rule of mixture and Halpin–Tsai equations as follows [58]:

$$E_{11} = V_f E_{11-f} + V_{mCNT} E_{11-mCNT}$$

$$E_{11-mCNT} = \frac{\eta_1 (1 + 2\left(\frac{l_{CNT}}{h_{CNT}}\right)\gamma_{11} V_{CNT} E_m)}{1 - \gamma_{11} V_{CNT}} \quad (1)$$

where $E_{11-mCNT}$ and V_{m-CNT} denote the Young's modulus and volume fraction of carbon nanotube (CNT) particles mixed with resin. l_{CNT}, h_{CNT} and W_{CNT} are the length, thickness, and width of the carbon nanotube. V_{CNT} and V_f are the volume fraction of CNT and fiber, respectively, and E_m and E_{11-f} denote Young's modulus of resin and fiber, respectively. Also η_1, η_2 and η_3 are the coefficients of the equipment [59].

$$\frac{1}{E_{22}} = \frac{V_{m-CNT}}{E_{22-mCNT}} + \frac{V_f}{E_{22-f}} - V_f V_{m-CNT}$$

$$\times \begin{pmatrix} \frac{(\nu_f{}^2 E_{22-mCNT}/E_{22-f})}{V_f E_{22-f} + V_{m-CNT} E_{22-mCNT}} \\ \frac{\nu_{12-mCNT}^2 E_{22-f}}{E_{22-mCNT}} \\ \frac{V_f E_{22-f} + V_{m-CNT} E_{22-mCNT}}{2\nu_f \nu_{12-mCNT}} \\ \frac{V_f E_{22-f} + V_{m-CNT} E_{22-mCNT}}{} \end{pmatrix} \quad (2)$$

where $E_{22-mCNT}$ is the Young's modulus of carbon nanotube (CNT) particles mixed with resin that is defined as follows:

$$E_{22-mCNT} = \frac{\eta_2 (1 + 2\left(\frac{l_{CNT}}{h_{CNT}}\right)\gamma_{22} V_{CNT} E_m)}{1 - \gamma_{22} V_{CNT}} \quad (3)$$

$$\frac{1}{G_{12}} = \frac{V_{m-CNT}}{G_{12-mCNT}} + \frac{V_f}{G_{12-f}} \quad (4)$$

$$G_{12-mCNT} = \frac{\eta_3 G_m}{1 - \gamma_{11} V_{CNT}} \quad (5)$$

where $G_{12-mCNT}$ is the shear modulus of carbon nanotube particles mixed with resin, and also, G_{12-f} is the shear modulus of fiber and the coefficientsγ_{11}, γ_{22} and γ_{12} are calculated as follows:

$$\gamma_{11} = \frac{\left(\frac{E_{11-CNT}}{E_m}\right) - 1}{\left(\frac{E_{11-CNT}}{E_m}\right) + 2\left(\frac{l_{CNT}}{h_{CNT}}\right)}$$

$$\gamma_{22} = \frac{\left(\frac{E_{22-CNT}}{G_m}\right) - 1}{\left(\frac{E_{22-CNT}}{E_m}\right) + 2\left(\frac{W_{CNT}}{h_{CNT}}\right)} \quad (6)$$

$$\gamma_{12} = \frac{\left(\frac{G_{12-CNT}}{E_m}\right) - 1}{\left(\frac{G_{12-CNT}}{G_m}\right)}$$

Mass density and Poisson's ratio for CNT/Epoxy/fiber are obtained as:

$$\nu_{12-mCNT} = \nu_{12-CNT} \times V_{CNT} + \nu_m \times V_m \quad (7)$$

$$\rho_{mCNT} = \rho_{CNT} \times V_{CNT} + \rho_m \times V_m \quad (8)$$

$$\nu_{12} = \nu_{12-mCNT} \times V_{m-CNT} + \nu_f \times V_f \quad (9)$$

$$\rho = \rho_{m-CNT} \times V_{m-CNT} + \rho_f \times V_f \quad (10)$$

V_f and V_{m-CNT} are defined as the volume fraction of nanocomposite fibers and epoxy resin and are related to each other by the following formula:

$$V_m + V_{CNT} + V_f = 1 \quad (11)$$

Table 1 shows the mechanical properties of the honeycomb core, resin, and reinforcements, including SMA and CNT. Table 2 demonstrates the dependent material properties of CNT[60–62].

Table 1. The mechanical properties of the honeycomb core, resin, and reinforcements, including SMA and CNT in the present work

Materials	Mechanical properties
Aluminum honeycomb core	$\boldsymbol{E_{11} = 0.1Gpa, G_{12} = 0.038Gpa, \rho = \frac{100Kg}{m^3}, \nu = 0.33}$
Carbon fiber	$\boldsymbol{E_{11} = 233.05Gpa, E_{22} = 23.1Gpa, G_{12} = 8.96Gpa, \rho = \frac{1750Kg}{m^3}, \nu = 0.2}$
Epoxy resin	$\boldsymbol{E_m = 3.52 - 0.034T\ Gpa, \alpha = 45(1 + 0.0005\Delta T) * 10^{-6}\ K^{-1}, \rho = \frac{1150Kg}{m^3}}$ $\boldsymbol{T = T_0 + \Delta T\ and\ T_0 = 300K, \nu = 0.34}$
Carbon nanotube	$\boldsymbol{\rho = \frac{1400Kg}{m^3}, \nu = 0.34, l = 9.26nm, h = 0.067, w = 14.77nm}$
SMA	$\boldsymbol{E_{11} = 67\ Gpa, G_{12} = 26.3\ Gpa, \rho = \frac{6450Kg}{m^3}, \nu = 0.33}$

Table 2. Temperature-dependent material properties of CNT

Temperature (Kelvin)	$\boldsymbol{E_{11}^{CNT}(TPa)}$	$\boldsymbol{E_{22}^{CNT}(TPa)}$	$\boldsymbol{G_{12}^{CNT}(TPa)}$	$\boldsymbol{\alpha_{12}^{CNT}(*10^{-6}/K)}$	$\boldsymbol{\alpha_{22}^{CNT}(*10^{-6}/K)}$
300	5.6466	7.0800	1.9445	3.4584	5.1682
500	5.5308	6.9348	1.9643	4.5361	5.0189
700	5.4744	6.8641	1.9644	4.6677	4.8943

3. Governing Equations

3.1 Displacement Fields

The displacement fields of sinusoidal shear deformation theory (SSDT) are considered as follows [63–68]:

$$u(x,y,z,t) = u_0(x,t) - z\frac{\partial w_0(x,t)}{\partial x} + \frac{h}{\pi}\sin\left(\frac{\pi z}{h}\right)\psi(x,t)$$
$$v(x,y,z,t) = 0 \quad (12)$$
$$w(x,y,z,t) = w_0(x,t)$$

where $u_0(x,t)$, $w_0(x,t)$, and $\psi(x,t)$ are the axial and transverse displacements and slope of the beam. Using equations (2-10), the following strain-displacement relations for a sandwich beam are obtained as follows:

$$\varepsilon_x = \frac{\partial u(x,y,z)}{\partial x} = \frac{\partial u_0(x)}{\partial x} - z\frac{\partial^2 w_0}{\partial x^2} + \frac{h}{\pi}\sin\left(\frac{\pi z}{h}\right)\frac{\partial \psi_{(x)}}{\partial x}$$
$$\varepsilon_y = \frac{\partial v(x,y,z)}{\partial y} = 0$$
$$\varepsilon_z = \frac{\partial w(x,y,z)}{\partial z} = 0 \quad (13)$$
$$\gamma_{xy} = \frac{\partial u}{\partial y} + \frac{\partial v}{\partial x} = 0$$
$$\gamma_{yz} = \frac{\partial v}{\partial z} + \frac{\partial w}{\partial y} = 0$$
$$\gamma_{xz} = \frac{\partial u}{\partial z} + \frac{\partial w}{\partial x} = cos\left(\frac{\pi z}{h}\right)\psi_{(x)}$$

where ε_x, ε_y , $\varepsilon_z$are the normal strains and γ_{xy}, γ_{xz}, γ_{yz} denote the shear strains.

3.2 Strain Energy

The strain energy variation for the composite beam is calculated as follows[69]:

$$\delta U = \int (\sigma_x\, \delta\varepsilon_x + \tau_{xz}\delta\gamma_{xz})dV \quad (14)$$

where $\sigma_x$and τ_{xz} are the normal and shear stress for a sandwich beam, respectively.

Substituting Eq. (13) into Eq. (14), the following relation is obtained:

$$\delta U = \int \begin{pmatrix} \sigma_x \delta\left(\frac{\partial u_0(x)}{\partial x} - z\frac{\partial^2 w_0}{\partial x^2} + \frac{h}{\pi}\sin\left(\frac{\pi z}{h}\right)\frac{\partial \psi_{(x)}}{\partial x}\right) \\ +\tau_{xz}\delta cos\left(\frac{\pi z}{h}\right)\psi_{(x)} \end{pmatrix} dV \quad (15)$$

The resultant forces and moments are defined as:

$$N_x = \int \sigma_x\, dz\,, \quad M_x^b = \int \sigma_x\, z\, dz$$
$$Q_{xz} = \int \tau_{xz}\cos\left(\frac{\pi z}{h}\right) dz \quad (16)$$
$$the\ R = \int \sigma_x \frac{h}{\pi}\sin\left(\frac{\pi z}{h}\right) dz$$

where N_x, M_x^b are the axial and bending resultant forces, respectively. Also, Q_{xz} and R denote the higher shear and bending resultant forces, respectively.

Substituting Eq. (16) into Eq. (15), the following result is obtained:

$$\delta U = \begin{pmatrix} \int Q_{xz}\delta\psi_x\, dA - \int \frac{\partial N_x}{\partial x}\delta u_x\, dA \\ -\int \frac{\partial^2 M_x^b}{\partial x^2}\delta w\, dA - \int \frac{\partial R}{\partial x}\delta\psi_{(x)}\, dA \end{pmatrix} \quad (17)$$

3.3 Kinetic Energy

The variation of kinetic energy for the CNT/Epoxy/fiber sandwich beam is calculated as follows:

$$\delta T = \int \rho\left(\frac{\partial u}{\partial t}\delta\frac{\partial u}{\partial t} + \frac{\partial v}{\partial t}\delta\frac{\partial v}{\partial t} + \frac{\partial w}{\partial t}\delta\frac{\partial w}{\partial t}\right)dz\, dA \quad (18)$$

$$\delta T = \int \begin{pmatrix} I^{(0)}\left(\frac{\partial u}{\partial t}\delta\frac{\partial u}{\partial t} + \frac{\partial w}{\partial t}\delta\frac{\partial w}{\partial t}\right) \\ +I^{(1)}\left(\frac{\partial^2 u}{\partial x\,\partial t}\delta\frac{\partial w}{\partial t} + \frac{\partial^2 w}{\partial x\,\partial t}\delta\frac{\partial w}{\partial t}\right) \\ -I^{(2)}\left(\frac{\partial^3 w}{\partial x^2\,\partial t}\delta\frac{\partial w}{\partial t}\right) \\ +J^{(0)}\left(\frac{\partial u}{\partial t}\delta\frac{\partial \psi}{\partial t} + \frac{\partial \psi}{\partial t}\delta\frac{\partial u}{\partial t}\right) \\ -J^{(1)}\left(\frac{\partial^2 w}{\partial x\,\partial t}\delta\frac{\partial \psi}{\partial t}\right) \\ +J^{(2)}\left(\frac{\partial^2 \psi}{\partial x\,\partial t}\delta\frac{\partial w}{\partial t}\right) \\ +K^{(1)}\left(\frac{\partial \psi}{\partial t}\delta\frac{\partial \psi}{\partial t}\right) \end{pmatrix} dA \quad (19)$$

$$\left(I^{(0)}, I^{(1)}, I^{(2)}\right) = \int \rho_{(z)}\,(1, z, z^2)dz$$
$$\left(J^{(0)}, J^{(1)}, J^{(2)}\right) = \int \rho_{(z)}\frac{h}{\pi}\sin\left(\frac{\pi z}{h}\right)(1, z, z^2)dz \quad (20)$$
$$K^{(1)} = \int \rho_{(z)}\left(\frac{h}{\pi}\right)^2 \sin^2\left(\frac{\pi z}{h}\right) dz$$

3.4 External Work

The variation of the total external work, including transverse load (q_x) buckling load (P_{cr}) and axial load (H_x) can be formulated as:

$$\delta W_{ext} = -\int (q_x w + P_{cr}\frac{\partial w}{\partial x}\delta\left(\frac{\partial w}{\partial x}\right) + H_x \delta u) dA \quad (21)$$

$$P_{cr} = P_m + P_T \quad (22)$$

where H_x and q_x are extensive loads applied to the composite beam in the x and z directions, respectively. Also, $P_m$and P_T are the mechanical and thermal buckling loads, respectively.

3.5 Hamilton's Principle

The governing equations of motion are obtained based on Hamilton's principle, which is defined as follows[67]:

$$\delta\Pi = \int (\delta T - \delta U - \delta W_{ext}) dt = 0 \quad (23)$$

$$\int \delta\Pi dt = \iint \begin{pmatrix} \delta u(-I^{(0)}\frac{\partial^2 u}{\partial t^2} + I^{(1)}\frac{\partial^3 w}{\partial t^2\,\partial x} \\ -J^{(0)}\frac{\partial^2 \psi}{\partial t^2} + \frac{\partial N}{\partial x} + H_x) \\ +\delta w(-I^{(0)}\frac{\partial^2 w}{\partial t^2} - I^{(1)}\frac{\partial^3 u}{\partial t^2\,\partial x} \\ +I^{(2)}\frac{\partial^4 w}{\partial x^2\,\partial t^2} - J^{(2)}\frac{\partial^3 \psi}{\partial t^2\,\partial x} \\ +\frac{\partial^2 M_x}{\partial x^2} + q_x - P_{cr}\frac{\partial^2 w}{\partial x^2} \\ +\delta\psi(-J^{(0)}\frac{\partial^2 u}{\partial t^2} - J^{(1)}\frac{\partial^3 w}{\partial t^2\,\partial x} \\ -K^{(1)}\frac{\partial^2 \psi}{\partial t^2} + \frac{\partial R}{\partial x} - Q_{xz}) \end{pmatrix} dA dt = 0 \quad (24)$$

Using equation (24), the three governing equations of the five layers nanocomposite beam considering honeycomb core and CNTRC with SMA particles are obtained as follows:

$$\delta u: H_x = I^{(0)}\frac{\partial^2 u}{\partial t^2} - I^{(1)}\frac{\partial^3 w}{\partial t^2\,\partial x} + J^{(0)}\frac{\partial^2 \psi}{\partial t^2} - A^{(0)}\frac{\partial^2 u}{\partial x^2} + A^{(1)}\frac{\partial^3 w}{\partial x^3} - C^{(0)}$$

$$\delta w: q_x = I^{(0)}\frac{\partial^2 w}{\partial t^2} + I^{(1)}\frac{\partial^3 u}{\partial t^2\,\partial x} - I^{(2)}\frac{\partial^4 w}{\partial x^2\,\partial t^2} + J^{(2)}\frac{\partial^3 \psi}{\partial t^2\,\partial x} - A^{(1)}\frac{\partial^3 u}{\partial x^3} + A^{(2)}\frac{\partial^4 w}{\partial x^4} - C^{(1)}\frac{\partial^3 \psi}{\partial x^3} + P_{cr}\frac{\partial^2 w}{\partial x^2} \quad (25)$$

$$\delta\psi = -J^{(0)}\frac{\partial^2 u}{\partial t^2} + J^{(1)}\frac{\partial^3 w}{\partial t^2\,\partial x} - K^{(1)}\frac{\partial^2 \psi}{\partial t^2} + C^{(0)}\frac{\partial^2 u}{\partial x^2} - C^{(1)}\frac{\partial^3 w}{\partial x^3} + D^{(0)}\frac{\partial^2 \psi}{\partial x^2} - B^{(2)}\psi = 0$$

In Eq. (25), the coefficients are defined as follows:

$$A^{(i)} = \int E\, z^i\, dz\,, i = 0,1,2$$
$$B^{(2)} = \int G\, cos^2\left(\frac{\pi z}{h}\right) dz$$
$$C^{(i)} = \int E\frac{h}{\pi} z^i \sin\left(\frac{\pi z}{h}\right) dz\,, i = 0,1 \quad (26)$$
$$D^{(0)} = \int E(\frac{h}{\pi})^2 \sin^2(\frac{\pi z}{h})\, dz$$

4. Solution Method

Substituting the response of displacements into Eqs. (25) yields the stiffness, mass, and geometric stiffness of matrices as follows:

$$\begin{bmatrix} D_{11} & D_{12} & D_{13} \\ D_{21} & D_{22} & D_{23} \\ D_{31} & D_{32} & D_{33} \end{bmatrix} \begin{bmatrix} U_m \\ W_m \\ \psi_m \end{bmatrix} = \begin{bmatrix} H_m \\ q_m \\ 0 \end{bmatrix} \quad (27)$$

Where:

$$D_{11} = -I^{(0)}\omega^2 + A^{(0)}\left(\frac{m\pi}{L}\right)^2$$
$$D_{12} = I^{(1)}\omega^2\frac{m\pi}{L} - A^{(1)}\left(\frac{m\pi}{L}\right)^3$$
$$D_{13} = -J^{(0)}\omega^2 + C^{(0)}\left(\frac{m\pi}{L}\right)^2$$
$$D_{21} = I^{(1)}\omega^2\frac{m\pi}{L} - A^{(1)}\left(\frac{m\pi}{L}\right)^3$$
$$D_{22} = -I^{(0)}\omega^2 - I^{(2)}\omega^2\left(\frac{m\pi}{L}\right)^2 - P_{cr}\left(\frac{m\pi}{L}\right)^2 + A^{(2)}\left(\frac{m\pi}{L}\right)^4 \quad (28)$$
$$D_{23} = J^{(1)}\omega^2\frac{m\pi}{L} - C^{(1)}\left(\frac{m\pi}{L}\right)^3$$
$$D_{31} = -J^{(0)}\omega^2 + C^{(0)}\left(\frac{m\pi}{L}\right)^2$$
$$D_{32} = J^{(1)}\omega^2\frac{m\pi}{L} - C^{(1)}\left(\frac{m\pi}{L}\right)^3$$

$$D_{33} = K^{(1)}\omega^2 - D^{(0)}\left(\frac{m\pi}{L}\right)^2 - B^{(2)}$$

Therefore, the mass matrix $[M]$, bending stiffness matrix $[K]$ and geometric stiffness matrix $[K_p]$ are obtained as follows:

$$K = \begin{bmatrix} K_{11} & K_{12} & K_{13} \\ K_{21} & K_{22} & K_{23} \\ K_{31} & K_{32} & K_{33} \end{bmatrix} \tag{29}$$

Where:

$$\begin{aligned} K_{11} &= A^{(0)}\left(\frac{m\pi}{L}\right)^2,\ K_{12} = -A^{(1)}\left(\frac{m\pi}{L}\right)^3 \\ K_{13} &= C^{(0)}\left(\frac{m\pi}{L}\right)^2,\ K_{21} = -A^{(1)}\left(\frac{m\pi}{L}\right)^3 \\ K_{22} &= A^{(2)}\left(\frac{m\pi}{L}\right)^4,\ K_{23} = -C^{(1)}\left(\frac{m\pi}{L}\right)^3 \\ K_{31} &= C^{(0)}\left(\frac{m\pi}{L}\right)^2,\ K_{32} = -C^{(1)}\left(\frac{m\pi}{L}\right)^3 \\ K_{33} &= -D^{(0)}\left(\frac{m\pi}{L}\right)^2 \end{aligned} \tag{30}$$

$$M = \begin{bmatrix} I^{(0)} & -I^{(1)}\frac{m\pi}{L} & J^{(0)} \\ -I^{(1)}\frac{m\pi}{L} & I^{(0)} + I^{(2)}\left(\frac{m\pi}{L}\right)^2 & -J^{(1)}\frac{m\pi}{L} \\ J^{(0)} & -J^{(1)}\frac{m\pi}{L} & +K^{(1)} \end{bmatrix} \tag{31}$$

$$K_p = \begin{bmatrix} 0 & 0 & 0 \\ 0 & -P_{cr}\left(\frac{m\pi}{L}\right)^2 & 0 \\ 0 & 0 & 0 \end{bmatrix} \tag{32}$$

The natural frequency of a sandwich beam is written as:

$$\det([K] - \omega_m^2[M]) = 0 \tag{33}$$

The following matrix form is used to calculate the deflection due to the application of transverse force (F):

$$[K]\begin{bmatrix} U_m \\ W_m \\ \psi_m \end{bmatrix} = [F] \tag{34}$$

$$[F] = \begin{bmatrix} H_m \\ q_m \\ 0 \end{bmatrix}$$

To obtain the critical buckling load, we have:

$$\left|[K] + [K_p]\right| = 0 \tag{35}$$

5. Thermal Flux

In this section, the one-dimensional heat flux of the composite beam is investigated based on Fig. 2 as follows:

$$\frac{d}{dt}\left[-KA_1\frac{dT}{dx}\right]dx + hA_2(T - T_a) = 0 \tag{36}$$

where h is an empirical heat transfer coefficient$\left(\frac{J}{s}.m^2.K\right)$, $A_2$is the surface area of the beam $(A_2 = P\,dx, m^2)$, P is the perimeter of the beam(m), T_a is the ambient temperature(K) and K is the thermal conductivity of the solid $\left(\frac{J}{s}.m.K\right)$, A_2 is the cross-sectional area of the beam (m²) For constant K, A_1, A_2 and P, Eq. (36) yields:

$$\frac{d^2T}{dx^2} - \alpha^2 T = -\alpha^2 T_a \tag{37}$$

where $\alpha^2 = \frac{hP}{KA_1}$ is the ambient temperature.

By solving Eq. (37), the following result is obtained:

$$T(x) = Ae^{\alpha x} + Be^{-\alpha x} + T_a \tag{38}$$

where α is equal to the square root of the multiply h (an empirical heat transfer coefficient) by P (the perimeter of the beam) divided to the multiply K (the thermal conductivity of the solid) by A_1 (the cross-sectional area of the beam) in which Eq. (38), A and B are defined as follows:

$$\begin{aligned} A &= \frac{(T_2 - T_a) - (T_1 - T_2)e^{-\alpha L}}{e^{\alpha L} - e^{-\alpha L}} \\ B &= \frac{(T_1 - T_2)e^{\alpha L} - (T_2 - T_a)}{e^{\alpha L} - e^{-\alpha L}} \end{aligned} \tag{39}$$

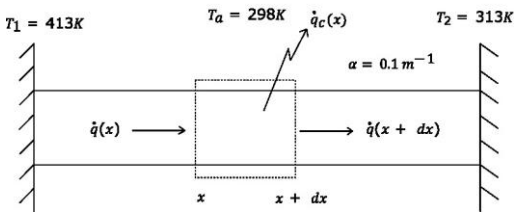

Fig. 2. A schematic view of steady heat conduction in a beam.

6. Validation

To validate the results, they are compared with existing literature by Thai [70] for EBBT,

TBT, and RBT in Tables 3 and 4. It is shown that the results of this article are in good agreement with other studies.

$$\bar{\omega} = \omega L^2 \sqrt{\frac{I^{(0)}}{EI}}, \bar{N} = \frac{N_{cr} L^2}{EI} \quad (40)$$

Table 3. Nondimensional fundamental frequency $\bar{\omega}$.

L/H	EBBT	TBT	RBT	Present work
5	9.7112	9.2740	9.2745	9.2618
10	9.8293	9.7075	9.7075	9.7067
20	9.8595	9.8281	9.8281	9.8281

Table 4. Nondimensional critical buckling load $\bar{N}$.

L/H	EBBT [10]	TBT	RBT	Present work
5	9.8696	8.9509	8.9519	8.9533
10	9.8696	9.6227	9.6228	9.6231
20	9.8696	9.8067	9.8067	9.8067

7. Results and Discussions

In this study, static bending, vibration, and buckling responses of a five layers nanocomposite sandwich beam considering honeycomb core, carbon nanotubes reinforced composite (Matrix and Resin) (CNTRC) in top and bottom of core, and also, shape memory alloy as well as matrix in top and bottom of CNTRC are investigated. Also, the influences of different parameters such as thickness ratio of core, V-CNT, V-SMA, and fiber orientation on deflection, natural frequency, and critical buckling force are studied.

Table 5. The efficiency coefficient for CNTs, mechanical and geometrical properties of carbon nanotubes, epoxy resin, fibers, and shape memory alloy

CNT, Matrix, and Fiber	SMA
$\boldsymbol{V_{CNT} = 0.11 \rightarrow \eta_1 = 0.149}$	$V_{SMA} = 0.01$
$\boldsymbol{\eta_2 = 0.934, \eta_3 = 0.934}$	$V_m = 0.99$
$\boldsymbol{V_{mCL} = 0.5}$	$H = 0.06\ m$
$\boldsymbol{V_f = 0.39}$	$q = -1000\ N/m^2$

Figure 3 shows the effect of volume fraction for carbon nanotube particles and the aspect ratio (L/H) of the sandwich beam on deflection, frequency, and buckling load. Increasing the volume fraction of carbon nanotube particles leads to an increase in the stiffness of the nanocomposite beam. Then, it increases the critical buckling load and natural frequency and reduces the deflection.

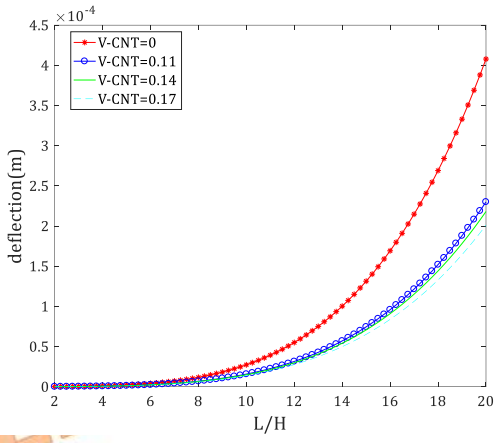

(a)

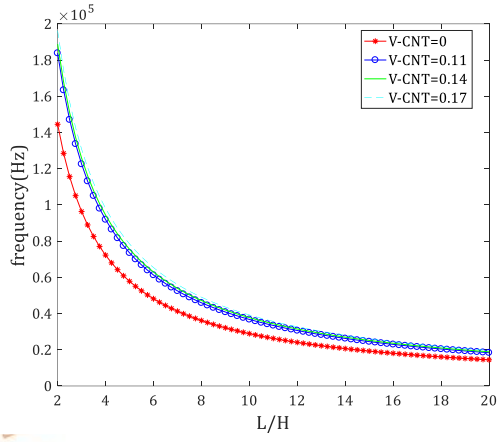

(b)

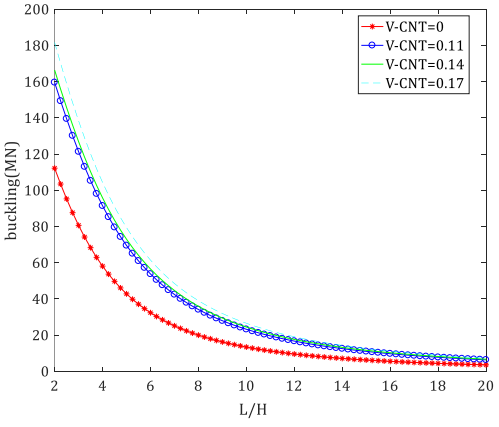

(c)

Fig. 3. Effect of volume fraction of carbon nanotube particles on (a) deflection, (b) natural frequency, (c) critical buckling load

Figure 4 shows the effect of volume fraction on the SMA-reinforced matrix of a sandwich beam. Although increasing V-SMA has a small effect on the beam's behavior, it reduces the deflection and increases the critical buckling load.

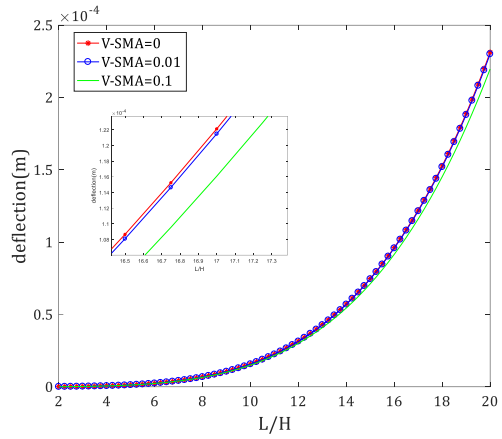

(a)

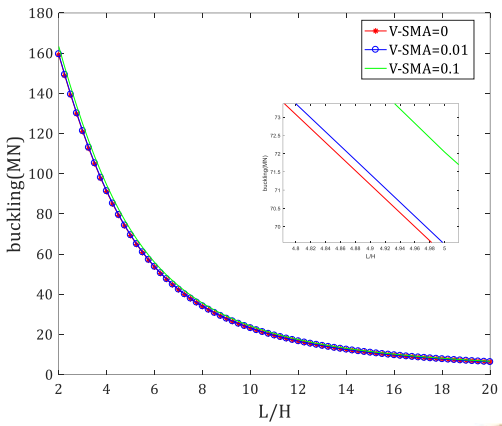

(b)

Fig. 4. Effect of volume fraction of SMA on (a) deflection ; (b) critical buckling load

Figure 5 shows the influence of fiber placement angles on composite beam behavior. The lowest deflection and highest natural frequency occur in mode $[0/0/0/0/0]_s$ and the highest deflection and lowest natural frequency occurs in mode $[90/90/90/90/90]_s$. The highest and lowest critical buckling loads happen in $L/H < 3$ respectively in case $[45/-45/45/-45/45]_s$ and $[90/90/90/90/90]_s$. If $3 \leq L/H \leq 12$, the maximum and minimum critical buckling load occurs in mode $[30/-30/30/-30/30]_s$ and $[90/-90/90/-90/90]_s$, respectively. Also, if $L/H > 12$ the maximum and minimum buckling load occurs in mode $[0/0/0/0/0]_s$ and $[90/-90/90/-90/90]_s$, respectively.

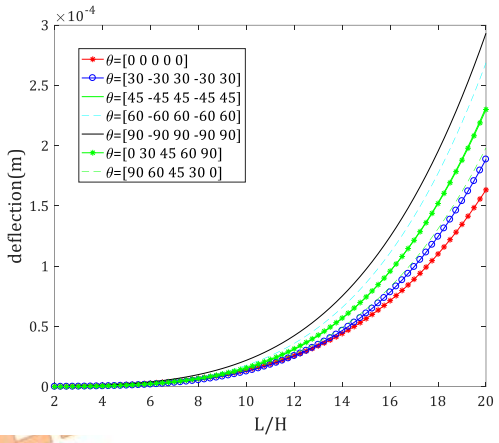

(a)

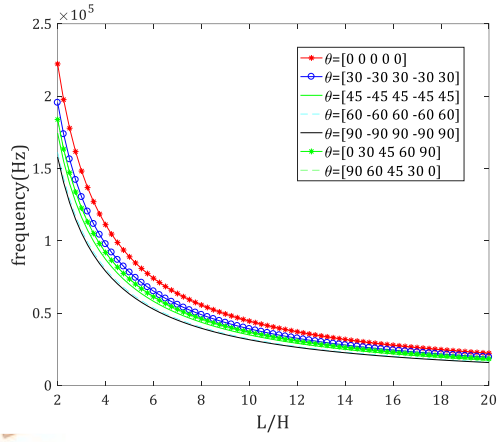

(b)

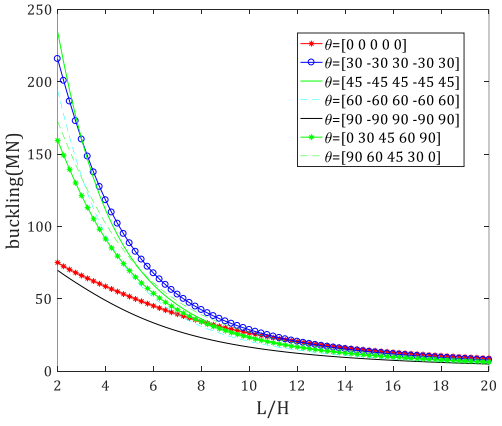

(c)

Fig. 5. Effect of fiber angles on (a) deflection, (b) natural frequency, (c) critical buckling load

Figure 6 shows the effect of the core on the total thickness ratio. Because the Young's modulus of the core is lower than the Young's modulus of carbon nanotube particles and shape memory alloy particles, by increasing h_c/H the equivalent stiffness decreases, according to Eqs. (29), (31), and (32), with a decrease in the stiffness matrix, the critical buckling load and natural frequency of the beam decrease, and the deflection of the beam increases.

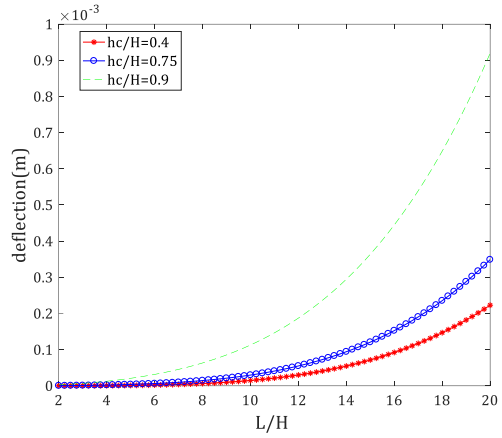

(a)

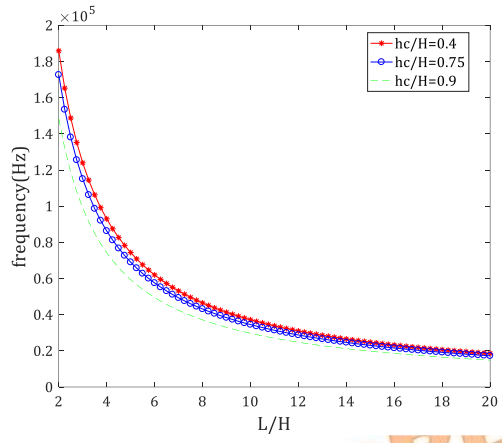

(b)

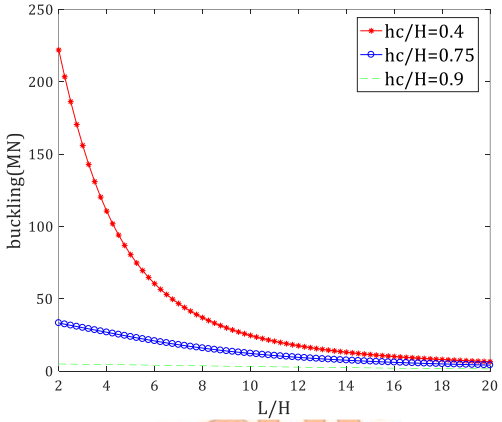

(c)

Fig. 6. Effect of core thickness on (a) Deflection

(b) Natural frequency; (c) critical buckling load

The distribution of temperatures along the length of the sandwich beam is shown in Fig. 7. It is shown that with an increase across the beam length, temperature based on boundary conditions decreases. Figure 8 shows the heat flux across the beam length for various thickness ratios. It is concluded that with an increase in thickness ratio, the thickness of the core increases, while the thickness of the face sheets decreases because the conductivity coefficient for CNT is higher than the core; thus, the heat flux across the beam length decreases. Figure 9 shows that with increasing temperature changes, the structure becomes softer, and the critical buckling load decreases.

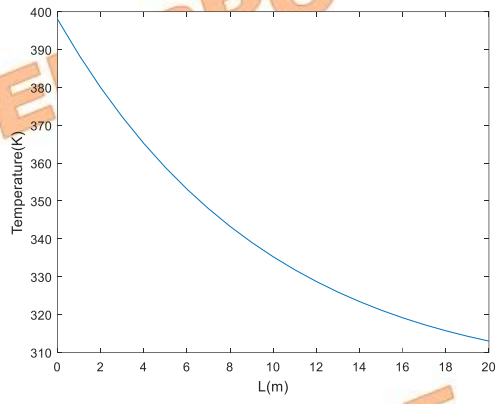

Fig. 7. Temperature variation along the length of the beam

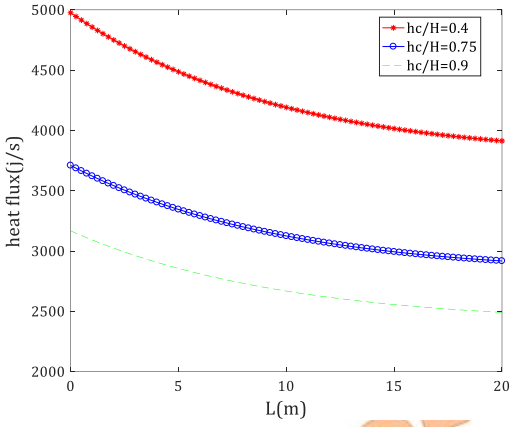

Fig. 8. The heat flux variation along the length of the beam for various thickness ratio

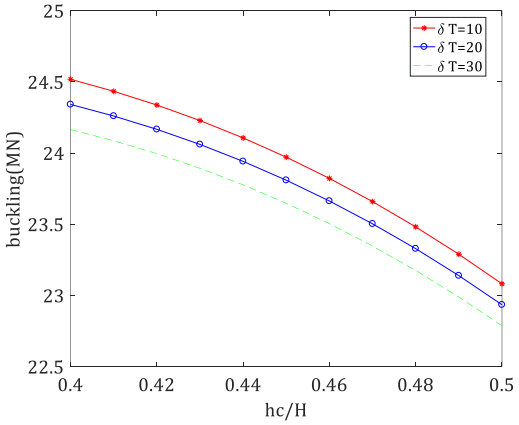

Fig. 9. The effect of temperature change on critical buckling load

8. Conclusions

This article investigated the vibration frequency, critical buckling load, and static bending of the five-layer composite beam of honeycomb core and carbon nanotubes reinforced with memory particles using the sinusoidal shear deformation theory. The governing equations of static equilibrium or motion were obtained using the principle of minimum potential energy and Hamilton's principle, respectively. The results of this research are stated as:

- Increasing the volume fraction of carbon nanotubes increases the vibration frequency and critical buckling load while decreasing beam deflection because the stiffness of a sandwich beam is enhanced.

- Increasing the volume fraction of SMA has very little effect on the deflection, vibration frequency, and critical buckling load of the beam.

- The lowest deflection and highest natural frequency occur in mode $[0/0/0/0/0]_s$ and the highest deflection and lowest natural frequency occur in mode $[90/90/90/90/90]_s$, the highest and lowest critical buckling loads happen in $L/H < 3$, respectively, in case $[45/-45/45/-45/45]_s$ and $[90/90/90/90/90]_s$. If $3 \leq L/H \leq 12$, the maximum and minimum critical buckling load occurs in mode $[30/-30/30/-30/30]_s$ and $[90/90/90/90/90]_s$,respectively. Also, if $L/H > 12$, the maximum and minimum buckling load occurs in mode $[0/0/0/0/0]_s$ and $[90/90/90/90/90]_s$,respectively.

- By increasing the ratio of the core thickness to the total thickness, the beam's vibration frequency and critical buckling load decrease, and the beam deflection increases because the sandwich beam becomes softer.

-The distribution of temperatures versus the length of the sandwich beam shows that with an increase across the beam length, temperature based on boundary conditions decreases.

- It is concluded that with an enhancement in thickness ratio, the heat flux decreases, it is due to increasing the thickness of the core; while the thickness of face sheets decreases, because the conductivity coefficient for CNT is higher than the core.

- It is shown that with increasing temperature changes, the structure becomes softer, and then the critical buckling load decreases.

Acknowledgments

The authors would like to thank the referees for their valuable comments and for increasing the quality of the present work. Also, the authors are thankful to the Iranian Nanotechnology Development Committee for supporting this research and the University of Kashan under Grant No. 1223097/5.

Conflict of Interest Statement

The author(s) declared no potential conflict of interest with respect to the research, authorship, and/or publication of this article.

Nomenclature

E	modulus of elasticity
G	shear modulus
ρ	Density
L	length
H	height
l	Length of CNT
h	thickness of CNT
w	width of CNT
η	efficiency parameter
V_f	volume fraction
$U_{(x,y,z,t)}$	axial displacements
$V_{(x,y,z,t)}$	axial displacements
$W_{(x,y,z,t)}$	transverse displacements
U	strain energy
W_{ext}	external energy
T	kinetic energy
$H_{(x)}$	longitudinal load
$q_{(x)}$	transverse load
P_{cr}	critical buckling load

References

[1] Mahesh, V. and Mahesh, V., 2024. Development and Mechanical Characterization of Light Weight Fiber Metal Laminate using Jute, Kenaf and Aluminium. *Mechanics of Advanced Composite Structures*, 11(2), pp.259–270. https://doi.org/10.22075/macs.2023.30686.1506.

[2] Amiri, F., Allaee, M.H. and Eskandari Jam, J., 2024. Experimental and Numerical Investigation of the Effect of Embedding Steel Wires inside the Foam of GFRP/Foam Sandwich Panel under Three-Point Bending Load. *Mechanics of Advanced Composite Structures*, 11(2), pp.271–280. https://doi.org/10.22075/macs.2023.31055.1526.

[3] Borah, P.P., Kashyap, S., Banerjee, S. and Kirtania, S., 2023. Modeling the Buckling Characteristics of Pineapple Leaf Fibre Reinforced Laminated Epoxy Composites. *Mechanics of Advanced Composite Structures*, 10(2), pp.233–246. https://doi.org/10.22075/macs.2022.28005.1425.

[4] Feli, S., Karimi, B. and Jafari, S.S., 2024. Analytical Modeling of Functionally Graded Carbon Nanotube-Reinforced Composite Plates under Low-Velocity Impact. *Mechanics of Advanced Composite Structures*, 11(2), pp.281–294. https://doi.org/10.22075/macs.2024.31101.1533.

[5] Ghorbanpour-Arani, A.A., Khoddami Maraghi, Z. and Ghorbanpour Arani, A., 2023. The Frequency Response of Intelligent Composite Sandwich Plate Under Biaxial In-Plane Forces. *Journal of Solid Mechanics*, 1(1), p.1. https://doi.org/10.22034/jsm.2020.1895607.1563.

[6] Ghorbanpour-Arani, A.H., Rastgoo, A., Sharafi, M.M., Kolahchi, R. and Ghorbanpour Arani, A., 2016. Nonlocal viscoelasticity based vibration of double viscoelastic piezoelectric nanobeam systems. *Meccanica*, 51(1), pp.25–40. https://doi.org/10.1007/s11012-014-9991-0.

[7] Arefi, M. and Zenkour, A.M., 2017b. Electro-magneto-elastic analysis of a three-layer curved beam. *Smart Structures and Systems*, 19(6), pp.695–703., https://doi.org/10.12989/sss.2017.19.6.695

[8] Arefi, M. and Zenkour, A., 2017a. Influence of micro-length-scale parameter and inhomogeneities on the bending, free vibration and wave propagation analyses of a FG Timoshenko's sandwich piezoelectric microbeam. *Journal of Sandwich Structures and Materials*, 21. https://doi.org/10.1177/1099636217714181.

[9] Ghorbanpour Arani, A., Jamali, M., Ghorbanpour-Arani, A., Kolahchi, R. and Mosayyebi, M., 2017. Electro-magneto wave propagation analysis of viscoelastic sandwich nanoplates considering surface effects. *Proceedings of the Institution of Mechanical Engineers, Part C: Journal of Mechanical Engineering Science*, 231(2), pp.387–403. https://doi.org/10.1177/0954406215627830.

[10] Zenkour, A.M., Arefi, M. and Alshehri, N.A., 2017. Size-dependent analysis of a sandwich curved nanobeam integrated with piezomagnetic face-sheets. *Results in Physics*, 7, pp.2172–2182. https://doi.org/10.1016/j.rinp.2017.06.032.

[11] Ghorbanpour-Arani, A.H., Rastgoo, A., Hafizi Bidgoli, A., Kolahchi, R. and Ghorbanpour Arani, A., 2017. Wave propagation of coupled double-DWBNNTs conveying fluid-systems using different nonlocal surface piezoelasticity theories. *Mechanics of Advanced Materials and Structures*, 24(14), pp.1159–1179. https://doi.org/10.1080/15376494.2016.1227488.

[12] Haghparast, E., Ghorbanpour-Arani, A. and Ghorbanpour Arani, A., 2020. Effect of Fluid–Structure Interaction on Vibration of Moving Sandwich Plate With Balsa Wood Core and Nanocomposite Face Sheets. *International Journal of Applied Mechanics*, 12, p.2050078. https://doi.org/10.1142/S1758825120500787.

[13] Arefi, M., Bidgoli, E.M.-R., Dimitri, R., Tornabene, F. and Reddy, J.N., 2019. Size-Dependent Free Vibrations of FG Polymer Composite Curved Nanobeams Reinforced with Graphene Nanoplatelets Resting on Pasternak Foundations. *Applied Sciences*, 9(8), p.1580. https://doi.org/10.3390/app9081580.

[14] Bargozini, F. and Mohammadimehr, M., 2024. The theoretical and experimental buckling analysis of a nanocomposite beams reinforced by nanorods made of recycled materials. *Polymer Composites*, 45(4), pp.3327–3342. https://doi.org/10.1002/pc.27993.

[15] Mohammadimehr, M. and Mehrabi, M., 2018. Electro-thermo-mechanical vibration and stability analyses of double-bonded micro composite sandwich piezoelectric tubes conveying fluid flow. *Applied Mathematical Modelling*, 60, pp.255–272. https://doi.org/10.1016/j.apm.2018.03.008.

[16] Nejadi, M.M., Mohammadimehr, M. and Mehrabi, M., 2021. Free vibration and stability analysis of sandwich pipe by considering porosity and graphene platelet effects on conveying fluid flow. *Alexandria Engineering Journal*, 60(1), pp.1945–1954. https://doi.org/10.1016/j.aej.2020.11.042.

[17] Babaeeian, M. and Mohammadimehr, M., 2020. Investigation of the time elapsed effect on residual stress measurement in a composite plate by DIC method. *Optics and Lasers in Engineering*, 128, p.106002. https://doi.org/10.1016/j.optlaseng.2020.106002.

[18] Yang, S.W., Hao, Y.X., Zhang, W., Ma, W.S. and Wu, M.Q., 2024. Nonlinear Frequency and Bifurcation of Carbon Fiber-Reinforced Polymer Truncated Laminated Conical Shell. *Journal of Vibration Engineering & Technologies*, 12(1), pp.457–468. https://doi.org/10.1007/s42417-023-00852-5.

[19] Di, H.-W., Fan, C., He, H., Zhang, N., Dong, J.-L. and Wang, Y.-T., 2023. A novel EVA-based composite via ceramization toward excellent flame retardance performance and high-temperature resistance. *Journal of Thermal Analysis and Calorimetry*. p. 11717-11726. https://doi.org/10.1007/s10973-023-12524-3.

[20] Shahedi, S. and Mohammadimehr, M., 2020. Vibration analysis of rotating fully-bonded and delaminated sandwich beam with CNTRC face sheets and AL-foam flexible core in thermal and moisture environments. *Mechanics Based Design of Structures and Machines*, 48(5), pp.584–614. https://doi.org/10.1080/15397734.2019.1646661.

[21] Mohammadimehr, M., Saidi, A.R., Ghorbanpour Arani, A., Arefmanesh, A. and Han, Q., 2011. Buckling analysis of double-walled carbon nanotubes embedded in an elastic medium under axial compression using non-local Timoshenko beam theory. *Proceedings of the Institution of Mechanical Engineers, Part C: Journal of Mechanical Engineering Science*, 225(2), pp.498–506. https://doi.org/10.1177/2041298310392861.

[22] Ong, O.Z.S., Ghayesh, M.H. and Losic, D., 2023. Vibrations of porous functionally graded CNT-reinforced viscoelastic beams connected via a viscoelastic layer. *International Journal of Engineering Science*, 191, p.103917. https://doi.org/10.1016/j.ijengsci.2023.103917.

[23] Baithalu, R. and Mishra, S.R., 2023. On optimizing shear rate analysis for the water-based CNT micropolar nanofluids via an elongating surface: response surface methodology combined with ANOVA test. *Journal of Thermal Analysis and Calorimetry*, 148, pp. 14275–14294 https://doi.org/10.1007/s10973-023-12567-6.

[24] Heidary, Z., Ramezani, S.R. and Mojra, A., 2023. Exploring the benefits of functionally graded carbon nanotubes (FG-CNTs) as a platform for targeted drug delivery systems. *Computer Methods and Programs in Biomedicine*, 238, p.107603. https://doi.org/10.1016/j.cmpb.2023.107603.

[25] Heidary, Z. and Mojra, A., 2021. Numerical Study of Thermal Effect on the Stability of Carbon Nanotubes Resting on a Viscoelastic Foundation Subjected to Magnetic Field. *International Journal of Structural Stability and Dynamics*, 22. https://doi.org/10.1142/S0219455422500249.

[26] Zhu, B., Chen, X., Dong, Y. and Li, Y., 2019. Stability analysis of cantilever carbon nanotubes subjected to partially distributed tangential force and viscoelastic foundation. *Applied Mathematical Modelling*, 73, pp.190–209. https://doi.org/10.1016/j.apm.2019.04.018.

[27] Kordzadeh, A., Zarif, M. and Amjad-Iranagh, S., 2023. Molecular dynamics insight of interaction between the functionalized-carbon nanotube and cancerous cell membrane in doxorubicin delivery. *Computer Methods and Programs in Biomedicine*, 230, p.107332. https://doi.org/10.1016/j.cmpb.2022.107332.

[28] Maleki, R., Afrouzi, H.H., Hosseini, M., Toghraie, D. and Rostami, S., 2020. Molecular dynamics simulation of Doxorubicin loading with N-isopropyl acrylamide carbon nanotube in a drug

delivery system. *Computer Methods and Programs in Biomedicine*, 184, p.105303. https://doi.org/10.1016/j.cmpb.2019.105303.

[29] Dilimon, V. and Shibli, S.M.A., 2022. Application of Surface Modified Carbon Nanotubes in Fuel Cells. pp.121–150. https://doi.org/10.1021/bk-2022-1425.ch006.

[30] Garg, A., Chalak, H.D., Zenkour, A.M., Belarbi, M.-O. and Sahoo, R., 2022. Bending and free vibration analysis of symmetric and unsymmetric functionally graded CNT reinforced sandwich beams containing softcore. *Thin-Walled Structures*, 170, p.108626. https://doi.org/10.1016/j.tws.2021.108626.

[31] Ghorbanpour Arani, A., Haghparast, E. and Ghorbanpour Arani, A. h., 2016. Size-dependent vibration of double-bonded carbon nanotube-reinforced composite microtubes conveying fluid under longitudinal magnetic field. *Polymer Composites*, 37(5), pp.1375–1383. https://doi.org/10.1002/pc.23306.

[32] Li, A., Xie, M., Yang, Y., Zhang, J., Wang, S., Chen, Y. and Zhou, W., 2022. Effect of CNTs content on the mechanical and arc-erosion performance of Ag-CNTs composites. *Diamond and Related Materials*, 128, p.109211. https://doi.org/10.1016/j.diamond.2022.109211.

[33] Zhang, D., Huang, Y. and Chia, L., 2022. Effects of carbon nanotube (CNT) geometries on the dispersion characterizations and adhesion properties of CNT reinforced epoxy composites. *Composite Structures*, 296, p.115942. https://doi.org/10.1016/j.compstruct.2022.115942.

[34] Arshadi, K. and Arefi, M., 2023. Out-of-Plane Strain Included Formulation for Free Vibration and Bending Analyses of a Sandwich GPL-Reinforced Microbeam Based on the MCST. *Journal of Vibration Engineering & Technologies*, 11(5), pp.2199–2214. https://doi.org/10.1007/s42417-022-00698-3.

[35] Ghorbanpour Arani, A., Mobarakeh, M.R., Shams, Sh. and Mohammadimehr, M., 2012. The effect of CNT volume fraction on the magneto-thermo-electro-mechanical behavior of smart nanocomposite cylinder. *Journal of Mechanical Science and Technology*, 26(8), pp.2565–2572. https://doi.org/10.1007/s12206-012-0639-5.

[36] Wang, G., Yao, S., Zhang, J., Han, C. and Zhang, H., 2023. Interlaminar performance of 3D CNTs/carbon black film enhanced GFRP under low-temperature cycling. *Journal of Alloys and Compounds*, 947, p.169595. https://doi.org/10.1016/j.jallcom.2023.169595.

[37] Fulmali, AO., Patnaik, S., Rathore, DK., Bhattacharjee, D., Gwalani, B., Ray, BC., Prusty, RK., 2023. Enhanced extreme temperature bending and delamination resistance of GFRP composites through z-directional aligned nano-reinforcement: Emphasizing the effects of CNT functionalization. *Composites Science and Technology*, 244, p.110272. https://doi.org/10.1016/j.compscitech.2023.110272.

[38] Ghorbanpour-Arani, A.H., Abdollahian, M. and Ghorbanpour Arani, A., 2020. Nonlinear dynamic analysis of temperature-dependent functionally graded magnetostrictive sandwich nanobeams using different beam theories. *Journal of the Brazilian Society of Mechanical Sciences and Engineering*, 42(6), p.314. https://doi.org/10.1007/s40430-020-02400-8.

[39] Arefi, M. and Zenkour, A.M., 2018a. Free vibration analysis of a three-layered microbeam based on strain gradient theory and three-unknown shear and normal deformation theory. *Steel and Composite Structures*, 26(4), pp.421–437. https://doi.org/10.12989/scs.2018.26.4.421

[40] Arefi, M. and Zenkour, A.M., 2017d. Transient analysis of a three-layer microbeam subjected to electric potential. *International Journal of Smart and Nano Materials*, 8(1), pp.20–40. https://doi.org/10.1080/19475411.2017.1292967.

[41] Arefi, M. and Zenkour, A.M., 2017c. Size-dependent vibration and bending analyses

of the piezomagnetic three-layer nanobeams. *Applied Physics A*, 123(3), p.202. https://doi.org/10.1007/s00339-017-0801-0.

[42] Arefi, M. and Najafitabar, F., 2021. Buckling and free vibration analyses of a sandwich beam made of a soft core with FG-GNPs reinforced composite face-sheets using Ritz Method. *Thin-Walled Structures*, 158, p.107200. https://doi.org/10.1016/j.tws.2020.107200.

[43] Qiang, X., Chen, L., Jiang, X. and Dong, H., 2023. Experimental study on anchorage and activation performance of Fe-SMA strips for structural reinforcements. *Construction and Building Materials*, 401, p.132961. https://doi.org/10.1016/j.conbuildmat.2023.132961.

[44] Yan, L., Li, Y., Chang, W.-S. and Huang, H., 2023. Seismic control of cross laminated timber (CLT) structure with shape memory alloy-based semi-active tuned mass damper (SMA-STMD). *Structures*, 57, p.105093. https://doi.org/10.1016/j.istruc.2023.105093.

[45] Asadi, H., Kiani, Y., Shakeri, M. and Eslami, M.R., 2014. Exact solution for nonlinear thermal stability of hybrid laminated composite Timoshenko beams reinforced with SMA fibers. *Composite Structures*, 108, pp.811–822. https://doi.org/10.1016/j.compstruct.2013.09.010.

[46] Kazem, A., Mehdi, M., Mostafa, B. and Timon, R., 2020. Free and forced vibration analysis of a sandwich beam considering porous core and SMA hybrid composite face layers on Vlasov's foundation. *Acta Mechanica*, 231(8), pp.3199–3218. https://doi.org/10.1007/s00707-020-02697-5.

[47] Vishal, P., Kaliperumal, D. and Padhi, R., 2018. Active Vibration Suppression of Nonlinear Cantilever Beam using Shape Memory Alloy Actuators. *IFAC-PapersOnLine*, 51(1), pp.130–135. https://doi.org/10.1016/j.ifacol.2018.05.022

[48] Garafolo, N.G. and McHugh, G., 2018. Vibration Control of a Flexible Beam with Embedded Shape Memory Alloy Wire. *Journal of Mechanical Design and Vibration*, 6(1), pp.9–16. https://doi.org/10.12691/jmdv-6-1-2.

[49] Rocha, J., Pereira, E. and Sena-Cruz, J., 2023. Feasibility of mechanical post-tensioning of annealed glass beams by activating externally bonded Fe-SMA reinforcement. *Construction and Building Materials*, 365, p.129953. https://doi.org/10.1016/j.conbuildmat.2022.129953.

[51] Viet, N.V. and Zaki, W., 2021. Bending model for functionally graded porous shape memory alloy/poroelastic composite cantilever beams. *Applied Mathematical Modelling*, 97, pp.398–417. https://doi.org/10.1016/j.apm.2021.03.058.

[52] Lu, Y., Jiang, J., Zhang, J., Zhang, R., Zhang, Q., Zhou, Y., Wang, L. and Yue, H., 2022. A dynamic stiffness improvement method for thin plate structures with laminated/embedded shape memory alloy actuators. *Thin-Walled Structures*, 175, p.109286. https://doi.org/10.1016/j.tws.2022.109286.

[53] Samadpour, M., Sadighi, M., Shakeri, M. and Zamani, H.A., 2015. Vibration analysis of thermally buckled SMA hybrid composite sandwich plate. *Composite Structures*, 119, pp.251–263. https://doi.org/10.1016/j.compstruct.2014.08.042.

[54] Park, J.-S., Kim, J.-H. and Moon, S.-H., 2004. Vibration of thermally post-buckled composite plates embedded with shape memory alloy fibers. *Composite Structures*, 63(2), pp.179–188. https://doi.org/10.1016/S0263-8223(03)00146-6.

[55] Kuang, K.S.C., Quek, S.T. and Cantwell, W.J., 2013. Active control of a smart composite with shape memory alloy sheet using a plastic optical fiber sensor. *Sensors and Actuators A: Physical*, 201, pp.182–187. https://doi.org/10.1016/j.sna.2013.06.024.

[56] Khalili, S., Khalili, S.M.R., Farsani, R.E. and Mahajan, P., 2020. Flexural properties of sandwich composite panels with glass laminate aluminum reinforced epoxy facesheets strengthened by SMA wires. *Polymer Testing*, 89, p.106641. https://doi.org/10.1016/j.polymertesting.2020.106641.

[57] Nejati, M., Ghasemi-Ghalebahman, A., Soltanimaleki, A., Dimitri, R. and Tornabene, F., 2019. Thermal vibration analysis of SMA hybrid composite double curved sandwich panels. *Composite Structures*, 224, p.111035. https://doi.org/10.1016/j.compstruct.2019.111035.

[58] Rostami, H. and Jedari Salami, S., 2022. Large amplitude free vibration of sandwich beams with flexible core and FG Graphene Platelet Reinforced Composite (FG-GPLRC) face sheets based on extended higher-order sandwich panel theory. *Thin-Walled Structures*, 180, p.109999. https://doi.org/10.1016/j.tws.2022.109999.

[59] Mohammadimehr, M., Emdadi, M. and Navi, B., 2020. Dynamic stability analysis of microcomposite annular sandwich plate with carbon nanotube reinforced composite facesheets based on modified strain gradient theory. *Journal of Sandwich Structures and Materials*, p.109963621878277. https://doi.org/10.1177/1099636218782770.

[60] Lei, Z.X., Zhang, L.W. and Liew, K.M., 2015. Free vibration analysis of laminated FG-CNT reinforced composite rectangular plates using the kp-Ritz method. *Composite Structures*, 127, pp.245–259. https://doi.org/10.1016/j.compstruct.2015.03.019.

[61] Lei, Z.X., Liew, K. and Yu, J., 2013. Free vibration analysis of functionally graded carbon nanotube-reinforced composite plates using the element-free kp-Ritz method in thermal environment. *Composite Structures*, 106, pp.128–138. https://doi.org/10.1016/j.compstruct.2013.06.003.

[62] Mohammadimehr, M., Navi, B. and Ghorbanpour Arani, A., 2015. Modified strain gradient Reddy rectangular plate model for biaxial buckling and bending analysis of double-coupled piezoelectric polymeric nanocomposite reinforced by FG-SWNT. *Composites Part B: Engineering*, 87. https://doi.org/10.1016/j.compositesb.2015.10.007.

[63] Sarafraz, M., Seidi, H., Kakavand, F. and Viliani, N.S., 2023. Free vibration and buckling analyses of a rectangular sandwich plate with an auxetic honeycomb core and laminated three-phase polymer/GNP/fiber face sheets. *Thin-Walled Structures*, 183, p.110331. https://doi.org/10.1016/j.tws.2022.110331.

[64] Arefi, M. and Zenkour, A.M., 2018b. Size-dependent electro-elastic analysis of a sandwich microbeam based on higher-order sinusoidal shear deformation theory and strain gradient theory. *Journal of Intelligent Material Systems and Structures*, 29(7), pp.1394–1406. https://doi.org/10.1177/1045389X17733333.

[65] Arefi, M. and Zenkour, A.M., 2019. Influence of magneto-electric environments on size-dependent bending results of three-layer piezomagnetic curved nanobeam based on sinusoidal shear deformation theory. *Journal of Sandwich Structures & Materials*, 21(8), pp.2751–2778. https://doi.org/10.1177/1099636217723186.

[66] Arefi, M. and Zenkour, A.M., 2017e. Transient sinusoidal shear deformation formulation of a size-dependent three-layer piezo-magnetic curved nanobeam. *Acta Mechanica*, 228(10), pp.3657–3674. https://doi.org/10.1007/s00707-017-1892-6.

[67] Arefi, M. and Zenkour, A.M., 2018c. Thermal stress and deformation analysis of a size-dependent curved nanobeam based on sinusoidal shear deformation theory. *Alexandria Engineering Journal*, 57(3), pp.2177–2185. https://doi.org/10.1016/j.aej.2017.07.003.

[68] Bargozini, F., Mohammadimehr, M., Dawi, E.A. and Salavati-Niasari, M., 2024. Buckling of a sandwich beam with carbon nano rod reinforced composite and porous core under axially variable forces by considering general strain. *Results in Engineering*, 21, p.101945.

https://doi.org/10.1016/j.rineng.2024.101945.

[69] Arabzadeh-Ziari, M., Mohammadimehr, M., Arabzadeh-Ziari, E. and Asgari, M., 2024. Deflection, buckling and vibration analyses for a sandwich nanocomposite structure with foam core reinforced with GPLs and SMAs based on TSDBT. *Journal of Computational Applied Mechanics*, 55(2), pp.289–321. https://doi.org/10.22059/jcamech.2024.374370.1017.

[70] Thai, H.-T., 2012. A nonlocal beam theory for bending, buckling, and vibration of nanobeams. *International Journal of Engineering Science*, 52, pp.56–64. https://doi.org/10.1016/j.ijengsci.2011.11.011.